Journal of Marine Research, 55, 861–883, 1997

Agulhas ring dynamics from TOPEX/POSEIDON satellite altimeter data

by Gustavo J. Goni[1], Silvia L. Garzoli[2], Andreas J. Roubicek[3], Donald B. Olson[1] and Otis B. Brown[1]

ABSTRACT

The transfer of warm water from the Indian Ocean into the South Atlantic subtropical gyre takes place in the form of rings and filaments formed when the Agulhas Current retroflects south of Africa between 15 and 25E. A survey of the rings formed from September 1992 until December 1995 in the Retroflection region was carried out using TOPEX/POSEIDON altimeter data. A two-layer model was used to estimate the upper layer thickness from the altimeter-derived sea-surface height anomaly data. An objective analysis scheme was used to construct a map of upper layer thickness every ten days. Seventeen rings and their trajectories were identified using these maps. The shedding of rings from the Agulhas Current was neither continuous nor periodic, and for long periods there is no formation of rings. Several rings remained in the region for more than a year and, at any given time, 2 to 6 rings coexisted in the region east of the Walvis Ridge. The results showed that the number of rings translating simultaneously in this region is larger during the first half of each year. The upper layer transport of the Agulhas Current in the Retroflection region was computed and a close association between high variations in transport and ring shedding was found. Rings translated WNW at translation speeds ranging from 5 to 16 km day^{-1} following formation. The values of available potential energy computed for the rings place them among the most energetic rings observed in the world oceans, with values of up to 70×10^{15} J. Transport computations indicate that each ring contributes in the average approximately 1 Sv of Agulhas Current waters to the Benguela Current.

1. Introduction

The Agulhas Current is a western boundary current that carries South Indian Subtropical Central Water southward and parallel to the southeastern African coast. After turning to the west, the circulation of this current turns or retroflects back to the east between 15 and 25E (Harris and van Foreest, 1978). The upper ocean dynamics indicate an interocean transfer of warm waters into the South Atlantic, and of cold waters into the Indian Ocean (Lutjeharms and Valentine, 1988). This process occurs when waters of the Agulhas Current

1. Division of Meteorology and Physical Oceanography, Rosenstiel School of Marine and Atmospheric Science, University of Miami, 4600 Rickenbacker Causeway, Miami, Florida, 33149, U.S.A.

2. NOAA/AOML, 4301 Rickenbacker Causeway, Miami, Florida, 33149, U.S.A. (on leave from Lamont Doherty Earth Observatory, Columbia University, Palisades, New York, 10964, U.S.A.)

3. Cooperative Institute for Marine and Atmospheric Studies (CIMAS), Rosenstiel School of Marine and Atmospheric Science, University of Miami, 4600 Rickenbacker Causeway, Miami, Florida, 33149, U.S.A.

shed rings and filaments into the South Atlantic (Duncan, 1965; Harris and van Foreest, 1978; Gordon, 1985). Warm-core anticyclonic Agulhas rings dominate the eddy field to the west of the Agulhas Retroflection and are capable of producing most of the rest of the eddy field through radiation as they decay (Olson, 1991). These rings usually join the South Atlantic Subtropical gyre as part of the Benguela Current, the eastern boundary flow that drifts northward adjacent to southwest Africa. These Agulhas rings not only transfer warmer and saltier waters into that region, but are also a source of kinetic and potential energy (Olson and Evans, 1986). In addition to the fluid transferred in ring cores from the Indian to the Atlantic Ocean, rings act as diffusive elements through the production of filaments of fluid pulled across the mean geostrophic contours in the region. While this flux occurs both along and across the ring's trajectory, Dewar and Flierl (1985) have shown that the alongtrack component of this mixing, i.e. along the ring corridor, dominates in terms of flux.

A continuous monitoring of the ring formation and evolution in the Agulhas Retroflection region can be difficult to carry out using infrared and color imagery due to the persistent cloud coverage in the area (Lutjeharms and Van Ballegooyen, 1988). Moreover, the vast transfer of heat between the rings and the atmosphere makes the ring trajectories difficult to identify using infrared images, since the contrast in sea-surface temperature between the rings and their surrounding waters decreases as the rings translate westward (Olson *et al.,* 1992). Although the rings lose their surface signature in sea-surface temperature, they maintain their sea-surface height patterns. They can usually be identified as positive values of the sea-surface height anomaly (SHA), as they translate westward in the South Atlantic (Van Ballegooyen *et al.,* 1994; Byrne *et al.,* 1995), making altimeter data especially useful to study these mesoscale features.

Several studies have been carried out using hydrographic data (e.g. Duncombe Rae *et al.,* 1992; Van Ballegooyen *et al.,* 1994), GEOSAT data (e.g. Feron *et al.,* 1992; Gordon and Haxby, 1990; Byrne *et al.,* 1995) and data from inverted echosounders (Duncombe Rae *et al.,* 1996), to provide estimates of the translation speed and energy parameters of the rings. One of the first descriptions of the Retroflection region based on satellite infrared imagery observations has been provided by Lutjeharms (1981). GEOSAT altimetry later allowed the investigation of the formation of rings and their trajectories by providing a continuous coverage of the sea-surface height pattern in the region.

There are two major external factors that play an important role in modifying the size, shape and motion of rings: bottom topography and large-scale flow. Theoretical studies on the influence of bottom topography (Kamenkovich *et al.,* 1996) have indicated that the Walvis Ridge slows the speed of translation of the Agulhas rings before they reach the ridge. Lutjeharms and Valentine (1988) have confirmed this result by analyzing the influence of bottom topography on the dynamics of cold and warm rings in the Agulhas Retroflection region from infrared imagery and hydrographic observations. This effect has also been detected using altimeter data by Lutjeharms (1996). Theoretical studies have shown that a strong barotropic flow increases the translation speed of the rings (Dewar and

Gailliard, 1994). GEOSAT studies have shown that five to six Agulhas rings enter the Atlantic Ocean every year between 1987 and 1989, and that their translation speeds range from 5 to 10 km day^{-1} (Byrne *et al.*, 1995). Gordon and Haxby (1990) have also used GEOSAT altimeter data to follow the trajectory of seven rings from November 1986 to November 1987. This study estimated that the ring translation speed ranges from 5 to 7 km day^{-1}. Garzoli *et al.* (1996) have estimated the translation speed of rings at 30S using inverted echosounder data as 12.8 km day^{-1} and as 6 to 7 km day^{-1} near the Walvis Ridge. The mean speed of propagation of rings in the Agulhas Retroflection region has been estimated at 5 km day^{-1} using the lag correlation between time series collected from current meter records (Bottero, personal communication, 1996). Gründlingh (1995) used the first year of T/P data to track five anticyclonic rings formed in the Agulhas region. Agulhas rings have been observed as far south as 46S, farther south of the subtropical convergence (Lutjeharms and Van Ballegooyen, 1988). Some Agulhas rings have been tracked across the Atlantic Ocean with GEOSAT altimeter data (Gordon and Haxby, 1990; Byrne *et al.*, 1995). Gordon and Haxby (1990) have reported that some rings reach 30W, only a few hundred kilometers from the eastern border of the Brazil Current. Moreover, this study also used hydrographic data to estimate that the Indian Ocean water mass shed by the rings ranges from 10 to 15×10^6 m^3 s^{-1}. The mean available potential energy for 12 rings detected with altimeter data during the three-year GEOSAT experiment has been estimated as 18×10^{15} J (Byrne *et al.*, 1995).

From June 1992 until November 1993 five inverted echosounders (IES) and four moored current meters (CMM) were deployed in a region of the Southeastern Atlantic Ocean, as part of the Benguela Sources and Transports (BEST) program (Garzoli *et al.*, 1994). Garzoli and Gordon (1996) have used these IES and CMM data sets along with data from three hydrographic cruises to monitor the transport and to analyze the origin of the Benguela Current. These same data sets have been used to monitor anticyclonic rings created in the Agulhas Retroflection region, to study their dynamics and to compute their energy (Duncombe Rae *et al.*, 1996), and to place approximate geographic limits on the corridor where the Agulhas rings translate (Garzoli and Gordon, 1996).

Altimeter data have been successfully used to monitor transports in western boundary currents (Kelly, 1991; Qiu, 1992; Goni *et al.*, 1996). In the first part of this work (Garzoli *et al.*, 1997), the BEST moored instruments have been used to determine the relationship between the altimeter-derived sea-surface height and the upper layer thickness and the dynamic height anomalies. These results have been included in a two-layer model to estimate the reduced gravity and upper layer thickness, and to monitor the geostrophic transport and the interannual variability of the water sources of the Benguela Current for the period January 1993–December 1995. The analysis performed in this work has indicated that the dynamic height fields derived from the altimeter data are a good proxy to monitor the geostrophic transport, while the upper layer thickness has been successfully used to monitor the ring dynamics in the region. The goal of the present study is to provide estimates of the number of rings formed in the Agulhas Retroflection region, and to

monitor their size, distribution in time and space, trajectories, speed of translation, residence time, and energy using the upper layer thickness fields derived from expressions developed in the first part of this work from TOPEX/POSEIDON (T/P) altimeter data. This work also investigates the relationship between the transport of the Agulhas Current across 19E in the Retroflection region and the formation of rings.

2. TOPEX/POSEIDON Satellite altimeter data

a. Sea height variability

Mesoscale features can be identified from altimeter-derived data as deviations from the mean sea-surface height. Specifically, anticyclonic warm rings can usually be detected as positive alongtrack values of SHA. The analysis of T/P data is summarized in Garzoli *et al.* (1997). Figure 1a shows the T/P groundtracks in the region of study, which is limited by 0 to 20E and 25S to 45S, in the SE Atlantic Ocean, and where contiguous groundtracks are separated longitudinally by approximately 3 degrees. This figure also shows the rms SHA map for the southeastern Atlantic computed for the first three years of T/P data. The largest rms values, of approximately 50 cm, correspond to the high variability area in the Agulhas Retroflection region, where the extreme values of SHA are approximately 75 cm and −60 cm. Other areas of high sea surface height variability correspond to the regions of high ring activity. The area of smaller rms values in the south corresponds to the region affected mainly by the Antarctic Circumpolar Current (ACC).

Figures 1b and 1c show the alongtrack rms sea surface height values for the T/P groundtracks identified with the letters A and B, respectively, in Figure 1a. These two groundtracks run west of the Agulhas Retroflection region. In Figure 1b the shape of the rms curve, with a peak at 38S and different slopes at each side of the peak, is associated with the dynamics of the region. The location of the peak indicates that, along this given groundtrack, the mesoscale variability is the largest at approximately 38S. The slope of these rms curves decreases more rapidly to the north of the peak, a situation that can be produced, for instance, by the passage of a larger number of rings to the south than to the north of the peak value location. The region crossed by the ACC has very low rms values of approximately 8 cm. Similar features are observed in the rms curve that corresponds to groundtrack B (Fig. 1c). In this case the location of the rms peak is farther to the north, suggesting a ring translation in the SE-NW direction.

b. Space-time diagrams

Figure 1a shows two T/P groundtracks, A and B, that cross the region where most of the warm rings are formed. Figures 2a and 2b show the SHA space-time diagram from September 1992 to December 1995 for these two groundtracks. The values shown in these plots are of SHA, the deviation of the sea height from the mean sea-surface height. Therefore, caution must be taken when making comparisons between SHA values that correspond to different locations. However, at a fixed location, changes in SHA have the same values as changes in sea-surface height. The SHA values are later used to compute upper layer thickness maps which provide a good proxy to monitor the ring trajectories.

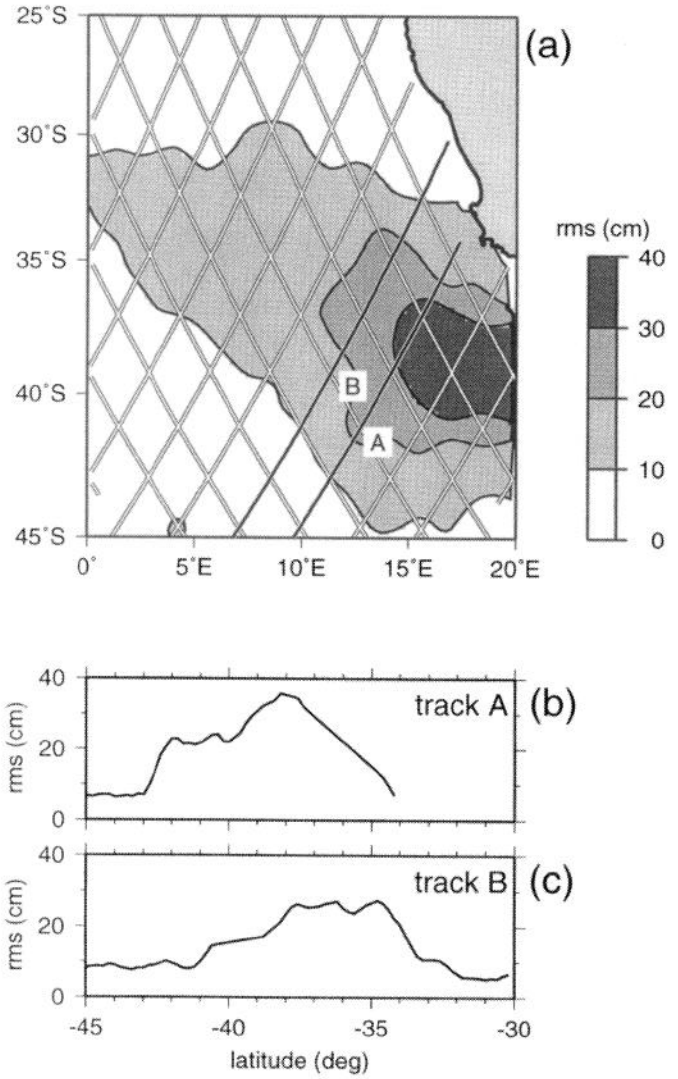

Figure 1. (a) Map of the region of study in the SE Atlantic Ocean showing the TOPEX/Poseidon (T/P) groundtracks. The figure also shows the root mean square variability, in centimeters, of the sea-surface height field derived from T/P data from September 1992 until December 1995. Higher values of variability are associated with the Agulhas Retroflection region and with anticyclonic ring dynamics. The alongtrack rms sea-surface height profiles for two selected groundtracks, A and B, are shown in Figure 1b and 1c, respectively.

These space-time SHA diagrams can provide a useful means to identify rings that cross an altimeter groundtrack. Anticyclonic warm rings crossing an altimeter groundtrack can usually be identified by their large positive SHA values, yellow and red colors in Figures 2a and 2b. Likewise, cyclonic cold rings can usually be identified by their large negative SHA

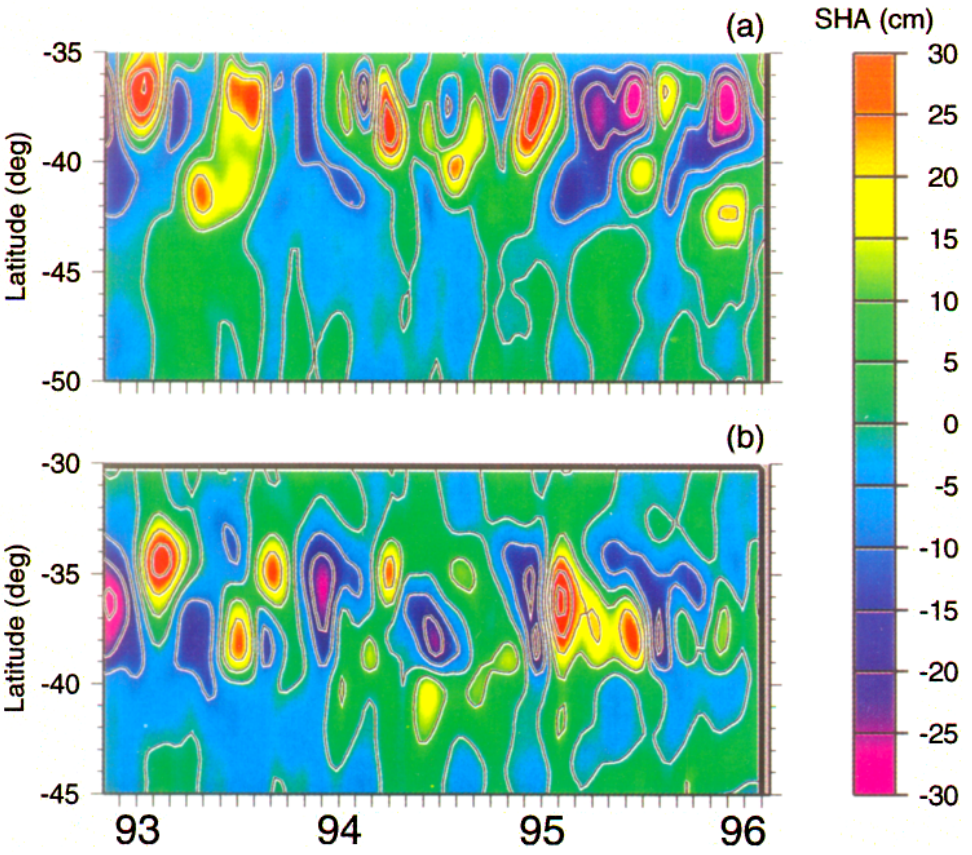

Figure 2. Space-Time diagrams of the sea surface height anomaly for the two T/P groundtracks shown in Figure 1a. (a) Diagram for T/P groundtrack A. (b) Diagram for T/P groundtrack B. The anticyclonic warm rings are characterized by higher values of sea-surface height anomaly. The cyclonic cold rings are associated with the lower values of anomaly.

values, dark blue and purple colors in the same figures. Since these two tracks cross the region west of the retroflection, the mesoscale features encountered in these two figures correspond to rings shed by the Agulhas Current and not by the eddy field associated with the borders of the Agulhas Current and Agulhas Return Current. On certain occasions anticyclonic and cyclonic rings alternate their passage through the altimeter groundtracks. This effect, known as recoil effect, has been first reported by Flierl (1977) and Mied and Lindemann (1979) for model results, and later confirmed by observations in the Gulf Stream by Hooker and Brown (1994). During the BEST experiment, Duncombe Rae *et al.* (1996) and Garzoli *et al.* (1996) observed a recoil effect in which the thermocline appears to shallow considerably after the passage of a ring before relaxing to the local mean. Figures 2a and 2b illustrate this effect by showing an alternation of high and very low sea surface height anomalies, probably due to the passage of cyclonic and anticyclonic rings.

However, as these values only represent anomalies, a more detailed analysis of the dynamics must be done to identify the cyclonic or anticyclonic character of these features. The general direction of the ring translation can be inferred by analyzing the SHA of adjacent altimeter groundtracks, like tracks A and B shown in Figure 1a. Most rings cross groundtracks A between 35S and 42S, and groundtrack B between 33S and 40S, indicating that rings move in a SE-NW direction.

Approximately 17 warm rings are identified crossing these two groundtracks during the three years of the analyzed T/P data. A similar number of rings have been identified entering this same region during the three years of the GEOSAT mission (Byrne *et al.*, 1995). As the rings are on occassion formed out of the range covered by groundtracks A and B, not all of them can be identified from the two space-time diagrams shown here. The largest SHA value, of almost 1 m, corresponds to one anticyclonic ring crossing track A during late 1992 at 36S. An eddy-like mesoscale feature, presumably an anticyclonic ring, with the largest negative SHA value also crosses this groundtrack at the same latitude during mid 1995, producing a sea surface height change of approximately -35 cm.

Small mesoscale features can sometimes be observed south of 42S. However, rings found south of this latitude have rather small length scales and sea-surface height signatures which cannot always be identified using altimeter data. Also, their trajectories cannot be very well detected as they move away from the region. The southernmost limit for a ring trajectory found from these two space-time diagrams is approximately 43S, north of the 46S limit set by Lutjeharms and Van Ballegooyen (1988).

3. Mean upper layer thickness and reduced gravity maps

In the present study the upper layer is considered to extend from the sea surface to the depth of the 10°C isotherm. Figure 3a shows the map of the mean upper layer thickness for the region of study, created using the Levitus climatological data (Levitus and Boyer, 1994). The mean upper layer thickness for this region is approximately 400 m. The area where the Agulhas Current retroflects is characterized by an increase of the mean upper layer thickness reaching values of around 460 m at around 37S. The region off the coast of southwest Africa has low mean upper layer thickness values, ranging from 300 to 375 m, due in part to the occurrence of upwelling. The Benguela Current produces an increase in the mean upper layer thickness in the SE-NW direction between 30S and 35S. The low values south of 37S are indicative of the presence of the Antarctic Circumpolar Current waters, where the thermocline sometimes reaches the sea surface. This map has the bathymetry superimposed. The major topographic feature in this region is the Walvis Ridge, which stretches from approximately 20S, 10E to 40S, 15W, with minimum depths of 1000 m.

Figure 3b shows the map of the reduced gravity, g', constructed using the available hydrographic data collected from the three BEST cruises (Duncombe Rae *et al.*, 1996). The mean reduced gravity value in the SE Atlantic obtained from this data set is 0.0108 m s^{-2}, with larger values of approximately 0.012 m s^{-2} observed in the Agulhas Retroflection

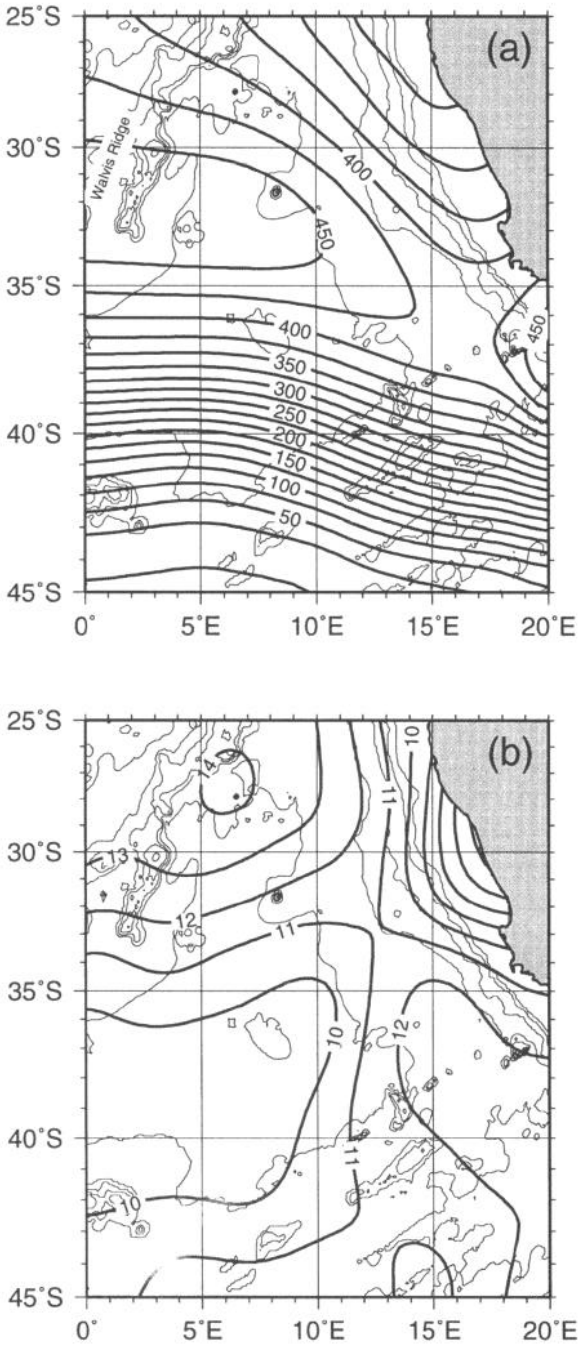

Figure 3. (a) Contours of the mean upper layer thickness derived from hydrographic observations obtained from the three BEST cruises. (b) Contours of $g' \times 100$, where g' is the reduced gravity. Larger values of g' are associated with stronger discontinuities in the vertical density profile.

region. Because the region shown in the map includes different dynamic regimes, the use of only one reduced gravity value for the whole area is not acceptable in computations of the upper layer thickness. Previous estimates of g' in this region include the work by Duncombe Rae *et al.* (1996) who have estimated its value in 0.0134 m s^{-2} from a regression between geopotential anomaly referred to the 1800 db level and the depth of the 10°C isotherm using historic and BEST hydrographic data. A slightly higher value has been obtained by Byrne *et al.* (1995), who have used a linear regression between the dynamic height anomaly referred to the 2000 db level and the depth of the 10°C isotherm.

4. Two-layer model

The upper layer and ring dynamics can be studied using the common two-layer model representation of the vertical structure of the ocean (Olson, 1991). The thermocline depth and the upper layer baroclinic and geostrophic transports can be estimated from the SHA values, provided that the mean upper layer thickness and the reduced gravity values are known in the region (Goni *et al.*, 1996). In the present study the interface between the two layers of different densities corresponds to the 10°C isotherm. For mesoscale features, such as rings or meanders, changes in sea level are compensated by changes in the upper layer thickness, plus a barotropic component. The slope of the curve obtained from a linear regression between the upper layer thickness anomaly and the sea surface height anomaly is proportional to the reduced gravity. The altimeter-derived upper layer thickness, $h_1(x, y, t)$, is then (Garzoli *et al.*, 1997):

$$h_1(x, y, t) = \overline{h_1}(x, y) + h_1'(x, y, t) = \overline{h_1}(x, y) + A(x, y)\eta'(x, y, t) + C(x, y), \quad (1)$$

where $\overline{h_1}(x, y)$ is the mean upper layer thickness, shown in Figure 3a, $h_1'(x, y, t)$ is the upper layer thickness anomaly, $\eta'(x, y, t)$ is the altimeter-derived sea surface height anomaly, and A and C are constants obtained from the reduced gravity, $g'(x, y)$, shown in Figure 3b, with C being proportional to the barotropic anomaly in the region. The details on how to apply the two layer model to the T/P data are given in part I of this work.

5. Results

a. Upper layer thickness maps

In the first part of this study the altimeter-derived SHA has proven to be a good proxy for monitoring the upper layer thickness anomaly in the Agulhas Retroflection region. An objective analysis scheme (Mariano and Brown, 1992) is used to interpolate the altimeter-derived SHA data onto a regular grid of 0.2 by 0.2 degrees and to create SHA maps every ten days. These interpolation maps are then used along with the mean upper layer thickness and mean reduced gravity maps to generate upper layer thickness maps every ten days. These maps are used to identify and track the rings formed in the region, as well as to estimate their speed of translation. The notation applied in this work to name each ring uses

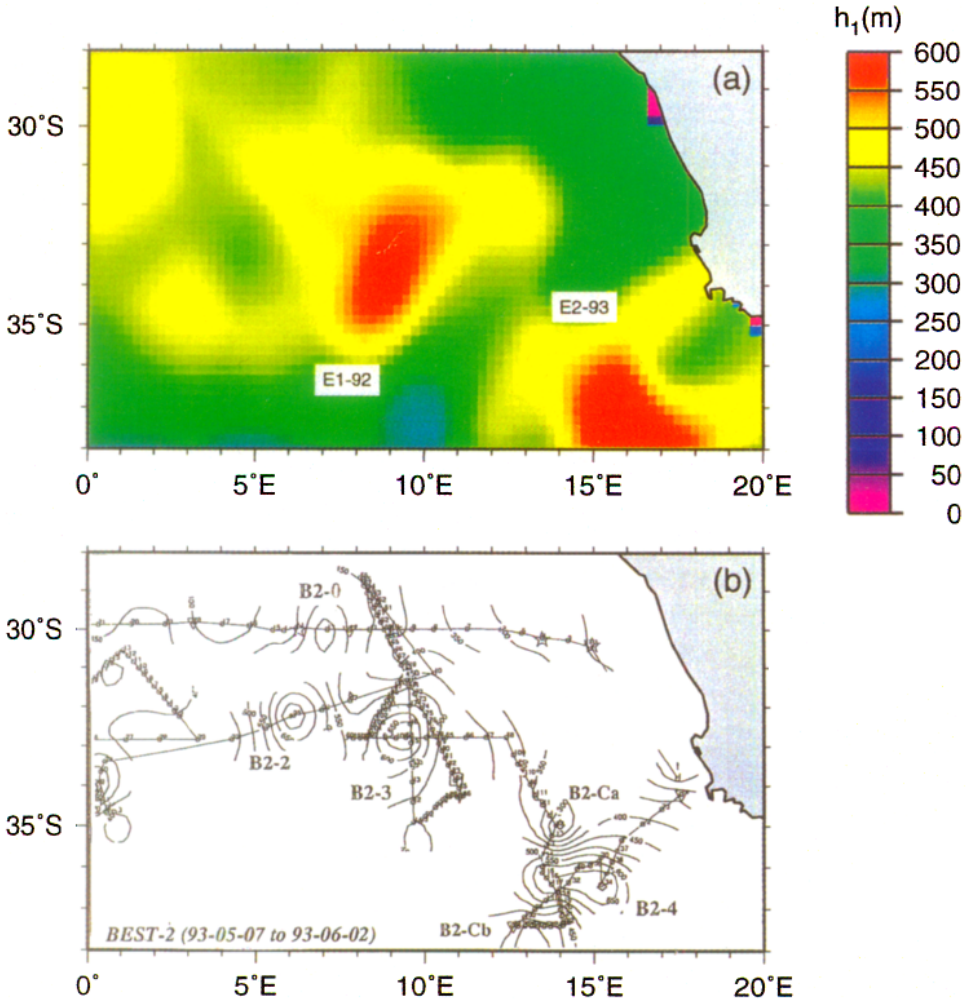

Figure 4. (a) OA-derived contours of upper layer thickness estimated using (1) during May 13–22, 1993, when two Agulhas rings, E1-92 and E2-93 are identified. (b) Hydrographically-derived contours of the depth of the 10°C isotherm for the period May 7–June 2, 1993 (Fig. 3 in Duncombe Rae *et al.,* 1996). The two Agulhas rings, B2-4 and B2-3, correspond to rings E2-93 and E1-92, respectively.

the letter E followed by a one digit number and the year in which the ring was first observed. For instance, ring E4-93 was the fourth ring formed during the year 1993.

Figure 4a shows the OA-derived h_1 color contours that correspond to the period May 13–22, 1993. These upper layer thickness values can be compared to actual hydrographic observations. Figure 4b shows the contours of the depth of the 10°C isotherm for the period May 7–Jun 2, 1993, derived from CTD/XBT observations obtained during the BEST-2 cruise (Fig. 3 in Duncombe Rae *et al.,* 1996). The three Agulhas rings (B2-2, B2-3 and

B2-4, in Duncombe Rae *et al.,* 1996) observed during the BEST-2 cruise are also detected by the altimeter, and shown in the color contours in Figure 4a. The differences between the OA-derived map and hydrographic observations, such as the small offset that exists between them, may be caused in part because the hydrographic data are taken over a period of one month while the h_1 map is a 10-day average, and because there also exists some subjectivity in the drawing of the hydrographic contours. From the BEST-2 hydrographic observations, rings B2-3 and B2-4 have maximum h_1 values of approximately 668 m and 710 m, respectively. The altimeter-derived estimates for rings B2-3 (E1-92) and B2-4 (E2-93), are 640 and 680 m, respectively. The location in Figure 4a of ring B2-2 is not very clear. Although this ring is identified by the altimeter data in a location close to that derived from hydrographic data (Fig. 4b), the very weak sea-height signature of ring B2-2 seems to produce values of upper layer thickness that are underestimated.

b. Ring dynamics

A total of 113 upper layer thickness maps, similar to the one shown in Figure 4a, are constructed using the T/P SHA data for the period October 1992–November 1995. These maps are used to visually identify the anticyclonic rings and their trajectories in the region of study. Agulhas rings are identified from these maps as regions of closed h_1 contours, with length scales larger than 0.5 degrees and with increasing h_1 toward their centers. The rings are followed along their paths across the area of study, and their locations, estimated with an error not larger than 1°, set at the point of maximum h_1. They are followed until they reach 0° of longitude or until they can no longer be tracked from the h_1 maps. A total of seventeen rings are identified using this criteria, with two rings formed at the end of 1992, five in 1993, four in 1994, and six in 1995. Most of the rings are identified as soon as they are formed in the Agulhas Retroflection region, around 15E. In contrast, the study by Byrne *et al.* (1995), identified only few rings east of 1E. This is because rings can be more easily identified and tracked from the h_1 maps than from the SHA data. Figures 5a through 5c show three maps with the trajectories of the fifteen rings formed during 1993, 1994 and 1995, respectively. Figure 5a also includes the two rings formed during November 1992. Figure 5d shows the map with the trajectory of the seventeen rings formed during the whole study period, with the topography contours superimposed. The crosses indicate the locations where the rings are first identified. The distance traveled by the ring in a month is denoted by the space between each symbol. These trajectories are computed using a 1-D Hermite interpolation of unevenly-spaced data, which guarantees that the trajectories pass through the altimeter-derived ring locations. The general tendency of the trajectories is in a SE-NW direction across the region. Rings E1-92 and E2-92 have also been detected by Gründling (1995) using the first year of T/P data. These rings, one unnamed and the other named A1 in his work, were formed by the division of one single ring (named A in his work), and remained in the region for almost a year.

Most of the rings seem to follow trajectories parallel to the isobath of 4000 m until reaching 2E after being shed by the Agulhas Current. The major topographic feature in the

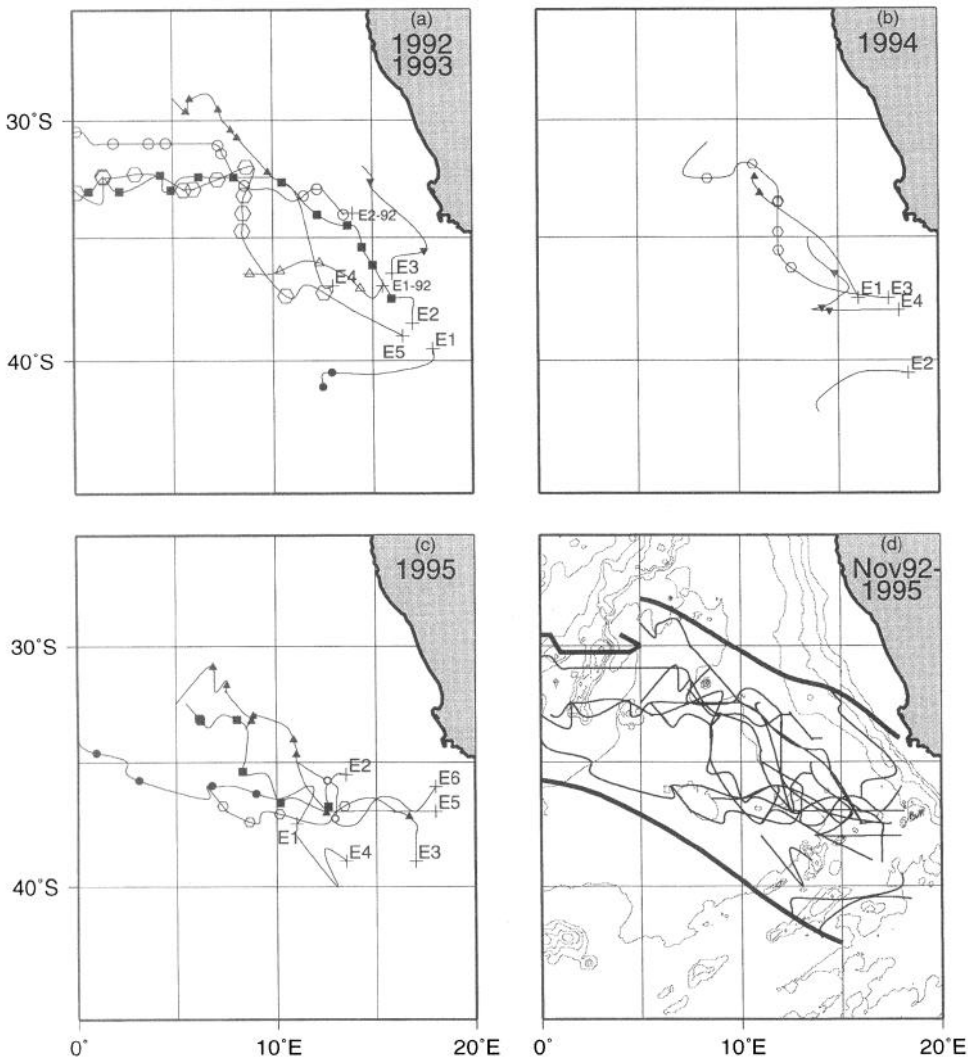

Figure 5. (a) Tracks of the anticyclonic Agulhas rings formed between November 1992 and December 1993. Two rings were formed in November 1992: E1-92 and E2-92. The rest of the rings in this figure were formed in 1993. The space between symbols indicate the distance traveled by the rings during a month. The crosses indicate the location where the warm rings are first observed. (b) Same as (a) except for year 1994. (c) Same as (a) except for year 1995. (d) Tracks of seventeen anticyclonic rings formed between November 1992 and December 1995, with the bathymetry superimposed. The ring corridor is indicated by thicker lines.

region of study is the Walvis Ridge (see Fig. 3a), with its minimum depth of around 1000 m located at approximately 30S, 6E. On average, it takes around a year for a ring to reach the Walvis Ridge. The five rings approaching this ridge appear to cross it over depths deeper than 2000 m, which is consistent with previous results on the effect of this ridge on ring

translation (Byrne *et al.*, 1995). However, some rings never reach the Walvis ridge. Rings that translate south of 38S, such as E1-93, E2-94 and E4-95, apparently become unstable and cannot be tracked for periods longer than three months. One ring, E3-93, has a trajectory more to the NE than any other ring, and can only be tracked for approximately two months.

The seventeen rings detected during the study period are used to determine an approximate ring corridor, constructed from the envelope of all the rings tracked in the region. The limits of this corridor are denoted by the heavy lines in the map of Figure 5. This ring corridor is in agreement with one that has been previously derived from hydrographic and IES data (Garzoli and Gordon, 1996).

Theoretical models of rings propagating in a region with bathymetric variations show that the rings undergo important changes in their shape as they translate (Dewar and Killworth, 1995). However, rings discussed in this work are assumed to be symmetrical and to have a Gaussian h_1 profile under the assumption that the bathymetry has not yet affected their shapes, soon after being shed. Therefore:

$$h_1(r) - h_\infty = h_0 e^{-r^2/2L^2}, \tag{2}$$

where r is the alongtrack distance measured from the center of the ring, $h_1(r)$ is the alongtrack depth of the 10°C isotherm across the ring, h_∞ is the depth of the 10°C isotherm far from the ring, L is the length scale, and h_0 is the maximum alongtrack depth of the ring measured from h_∞.

At the time when the rings are first identified from the upper layer thickness maps the parameters h_0, h_∞, and L are estimated by fitting (2) to the alongtrack altimeter-derived upper layer thickness profile (1) using a least square method. The shape of h_1 is represented by the radial distribution of the 10°C isotherm, as obtained from the altimeter-derived h_1 profiles using (1). A Gaussian curve is then fitted to the 10°C isotherm profile. These computations assume that the T/P groundtracks cross the rings through their centers. In general, the h_1 vs. alongtrack distance profiles are not symmetric because in most cases the ACC produces a very steep gradient and pronounced shallowing of the 10°C isotherm to the south. For this reason, h_∞ is determined from the northern half of the h_1 alongtrack profile. The least square nonlinear fit to the Gaussian function (2) is then performed by letting h_0 span a range of values between 150 and 400 m, and of L between 20 and 250 km.

The size of the rings can be quantified in terms of ring volume anomaly (*VOL*) (Olson, 1991). The *VOL* is that part of the ring volume with waters warmer than 10°C relative to h_∞, and is defined as (Olson and Evans, 1986):

$$VOL = \int_A (h_1(r) - h_\infty)\, dA, \tag{3}$$

where A is the area of the ring at h_∞. Assuming an alongtrack Gaussian profile of the upper layer thickness of the ring, the *VOL* is:

$$VOL = 2\pi L^2 h_0, \tag{4}$$

Table 1. Statistics of the parameters of the 17 anticyclonic rings shed by the Agulhas Current during the period November 1992–December 1995. The second column indicates the month and year when the rings were first detected from the altimeter data, *SHA* is the maximum alongtrack sea height anomaly, h_0 is the maximum upper layer thickness obtained from the gaussian fit, relative to the upper layer thickness of the waters surrounding the ring, h_∞; $h_1 = h_0 + h_\infty$ is the upper layer thickness; L is the radius of maximum velocity, *VOL* is the volume anomaly, *APE* is the available potential energy, V_{mean} is the mean translation speed, and *T* in the last column is the residence time in months.

Ring	Month of 1st observation	*SHA* (m)	h_0 (m)	h_∞ (m)	h_1 (m)	*L* (km)	*VOL* (10^{12} m^3)	V_{mean} (cm/s–km/day)	*APE* ($\times 10^{15}$ J)	*T* (months)
E1-92	Oct 92	0.60	258	396	654	107	19	6–5.2	13	12.5
E2-92	Oct 92	0.70	179	473	652	50	1	6–5.2	1	5
E1-93	Jan 93	0.92	428	190	618	80	17	8–6.9	20	3
E2-93	Mar 93	0.48	347	268	615	174	66	8–6.9	19	13
E3-93	Nov 93	0.10	81	342	423	122	8	6–5.2	2	2.5
E4-93	Dec 93	0.61	351	311	662	117	30	11–9.5	29	13
E5-93	Dec 93	0.26	198	303	501	103	13	6–5.2	7	7
E1-94	Feb 94	0.72	383	345	728	119	34	9–7.8	36	2.5
E2-94	Apr 94	0.85	354	198	552	181	73	18–15.6	71	1
E3-94	Jul 94	0.18	152	338	490	128	16	8–6.9	7	8
E4-94	Aug 94	0.51	322	332	654	83	14	7–6.0	12	4.5
E1-95	Jan 95	0.71	500	245	745	73	17	11–9.5	23	5
E2-95	Feb 95	0.39	288	302	590	160	46	8–6.9	37	7.5
E3-95	Mar 95	0.61	359	302	661	136	42	9–7.8	42	8.5+
E4-95	May 95	0.65	338	209	547	96	20	16–13.8	18	1
E5-95	Jun 95	0.30	223	313	536	87	11	8–6.9	7	5+
E6-95	Aug 95	0.27	185	345	530	147	25	11–9.5	13	3+
Average		0.52	291	306	597	116	26	9–7.8	24	

where *L*, the length scale of the Gaussian fit, also corresponds to the radius of maximum velocity (Duncombe Rae *et al.,* 1996).

The values of h_0, h_∞, *L* and *VOL*, along with the maximum sea height anomalies for each ring, are shown in Table 1. The mean value of *L* for the 17 observed rings is 116 km. The largest length scale factor, *L*, of 174 km corresponds to ring E2-93, which can be tracked for more than a year in the region. Duncombe Rae *et al.* (1996) report a slightly lower mean value of approximately 80 km for six rings observed during the BEST cruises. The maximum depth of a ring is $h_1 = h_0 + h_\infty$. The mean value of h_1 is approximately 600 m. The rings with the largest h_1 values of 730 m and 750 m are E1-94 and E1-95, respectively. The values of *VOL* range from 1 to 73 $\times$ 10^{12} m^3. Previous results estimated the *VOL* value for two Agulhas rings at 18 and 15 $\times$ 10^{12} m^3, and for the Gulf Stream warm core ring 82B at 3.9 $\times$ 10^{12} m^3 (Olson and Evans, 1986). The total *VOL* values are 134 $\times$ 10^{12}, 137 $\times$ 10^{12}, and 161 $\times$ 10^{12} m^3 year^{-1} during years 1993, 1994, and 1995, respectively. These results suggest that an average of 10^{14} m^3 (3 Sv) of Indian Ocean waters warmer than 10°C enters the South Atlantic Ocean in the form of rings every year. This is in agreement with

previously reported values obtained using Geosat and hydrographic data that estimated the mean volume of water warmer than 10°C in four rings to be around 0.2×10^{14} m^3 (Van Ballegooyen *et al.,* 1994).

A mean translation velocity, which is the combination of the ring velocity and the advective component due to the Benguela Current, is estimated for each ring by computing the mean ratio between traveled distances and times. The advective component has been reported to be no larger than half of the total translation velocity for rings studied in this same region using GEOSAT data (Byrne *et al.,* 1995). Models show that the motion of the ocean upper layer is highly influenced by the lower layer, and that rings with a large barotropic component move faster than baroclinic rings (Dewar and Gailliard, 1994). Numerical evidence of deep flow under Agulhas rings is also reported by Chassignet *et al.* (1990). Hydrographic observations have also shown that Agulhas rings have a very important deep structure (Duncombe Rae *et al.,* 1996), which can affect their speed of translation. The mean speed of translation for each ring is estimated directly from the movement of its location in the upper layer thickness maps. These mean speed values are also shown in Table 1. The fastest observed speed of 18 cm s^{-1} (16 km day^{-1}) corresponds to ring E2-94, making this velocity higher than any other reported ring translation speed value for this region. However, its high speed may be due to the ring being embedded in a strong current. The lowest mean translation speed of 6 cm s^{-1} (5 km day^{-1}) corresponds to rings E1-92, E3-93 and E5-93. Garzoli *et al.* have reported a mean translation speed value of 6 cm s^{-1} for ring E4-93 at 30S. The mean value computed here for this ring is 11 cm s^{-1} throughout the whole region. The mean translation speed for all the rings studied in this work is 9 cm s^{-1} (8 km day^{-1}). This value is similar to that calculated by Garzoli *et al.* (1996) of 12 km day^{-1} for several rings detected during the BEST experiment. The mean translation speed for all the rings is also within the range of translation speed values reported by Byrne *et al.* (1995) for rings detected using GEOSAT data. Rings have been reported to move faster when they translate over deep bathymetry than when they reach the Walvis ridge (Byrne *et al.,* 1995; Kamenkovich *et al.,* 1996; Lutjeharms, 1996). This effect can be visualized in Figures 5a through 5c, where distances between symbols are usually larger right after the rings are formed than when they approach the Walvis ridge. Three rings, E2-93, E5-93 and E1-95, cross the Walvis ridge south of 30S. Only one ring, E3-93, reaches the ridge north of this latitude. None of the four rings formed during 1994 seem to reach the ridge, as they cannot be traced for more than five months from the upper layer thickness maps.

c. *Energetics*

i. Eddy kinetic energy. The mesoscale eddy kinetic energy, or fluctuation from the mean kinetic energy, can be estimated in terms of the sea level variance field (Garrafo *et al.,* 1992). When the sea-surface height anomalies are referred to the arithmetic mean sea surface or other surface relatively close to it, the sea-surface height variance, σ_η^2, and the

sea-surface height anomaly variance, $\sigma^2_{\eta'}$, are the same. Therefore:

$$\sigma^2_{\eta} = \sigma^2_{\eta'} = \frac{1}{n}\sum_{i=1}^{n} (\eta')^2. \tag{5}$$

The upper layer current velocity in a y-direction perpendicular to an x-direction is:

$$v_y = \bar{v}_y + v'_y, \tag{6}$$

where $\bar{v}_y$ is the mean upper layer velocity and v'_y is the upper layer velocity anomaly or eddy upper layer velocity, defined as:

$$v'_y = \frac{g}{f}\frac{\partial \eta'}{\partial x}, \tag{7}$$

where g is the acceleration of gravity and f the Coriolis factor. The eddy upper layer velocity variance is:

$$\sigma^2_{v'_y} = \frac{1}{n}\sum_{i=1}^{n} (v'_y)^2, \tag{8}$$

Therefore:

$$\sigma^2_{v_y} = \frac{g^2}{f^2}\frac{1}{n}\sum_{i=1}^{n}\left(\frac{\partial \eta'}{\partial x}\right)^2. \tag{9}$$

Similarly, the variance of the velocity in the x-direction is:

$$\sigma^2_{v_x} = \frac{g^2}{f^2}\frac{1}{n}\sum_{i=1}^{n}\left(\frac{\partial \eta'}{\partial y}\right)^2. \tag{10}$$

The surface eddy kinetic energy per unit mass is then:

$$K_e = \tfrac{1}{2}[\sigma^2_{v_x} + \sigma^2_{v_y}]. \tag{11}$$

If the velocity variance is isotropic, this is $\sigma^2_{v_x} = \sigma^2_{v_y}$, then:

$$K_e = \sigma^2_{v_x}. \tag{12}$$

Figure 6 shows a map with the estimates of the surface eddy kinetic energy per unit mass using (11), with the bathymetric contours and the ring corridor superimposed. As expected, the Agulhas Retroflection region has the largest values of mesoscale kinetic energy. In this region most of the energy corresponds to the meandering of the Agulhas Current and ring formation, while the largest values outside this region are linked to ring activity. The values obtained for the first three years of T/P data are within the range of values obtained for the same region using the Semtner and Chervin model (Garrafo *et al.,* 1992). As expected, the

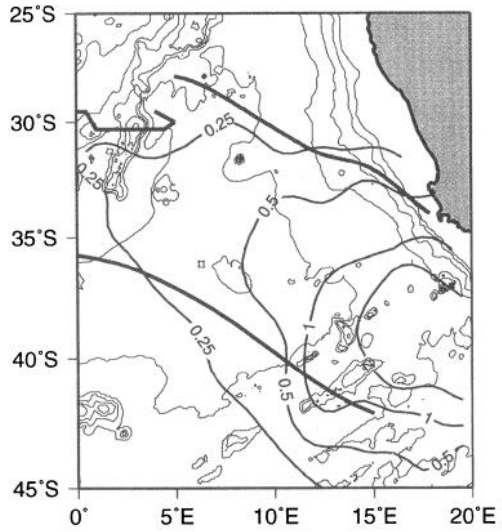

Figure 6. Eddy Kinetic Energy (K_e) in $m^2\ s^{-2}$ computed using T/P data. The higher values of energy are linked to the mesoscale processes in the Agulhas Retroflection region. The shape of the contours suggests a connection between the ring corridor, indicated by thicker lines, and K_e. The bathymetry is also shown.

ring corridor is closely linked to the eddy kinetic energy per unit mass contours, as the axis of the maximum eddy kinetic energy extends inside the ring corridor.

ii. Available potential energy. The intensity of the rings can be quantified in terms of ring energy content as available potential energy (*APE*) (Olson, 1991). The available potential energy (*APE*) is a quantity proportional to that part of the potential energy that can be converted into kinetic energy. The *APE* is defined as (Olson, 1991; Duncombe Rae *et al.*, 1996):

$$APE = \frac{1}{2}\rho_1 g' \int_A (h_1(r) - h_\infty)^2\, dA \tag{13}$$

where ρ_1 is the density of the upper layer. As in the volume anomaly derivation, an alongtrack Gaussian profile of the upper layer thickness of the ring is assumed. Therefore, the *APE* is:

$$APE = \frac{\pi}{2}\rho_1 g' h_0^2 L^2. \tag{14}$$

The estimated values of the *APE* for each ring are shown in Table 1. The initial *APE* for the rings just west of the Agulhas Retroflection region ranges from approximately 1×10^{15} J (ring E3-93) to 71×10^{15} J (ring E2-94), with a mean *APE* of 24×10^{15} J. This mean value is slightly higher than the 18×10^{15} J reported by Byrne *et al.* (1995) for a similar number

of rings tracked during the GEOSAT period. Other reported *APE* values are of approximately 30 and 50 $\times$ 10^{15} J for two Agulhas warm core rings (Olson and Evans, 1986). The *APE* values for rings E1-92 and E2-93 computed in this work are 13 and 20 $\times$ 10^{15} J, respectively. The *APE* of these two rings have been previously estimated at 7 and 23 $\times$ 10^{15} J by Duncombe Rae *et al.* (1996) (rings B2-3 and B2-4 in that work) using BEST data. The energy values of Agulhas rings are sometimes one order of magnitude larger than reported values for Gulf Stream rings (Joyce, 1984), and are only comparable to rings formed in the East Australian Current (Andrews and Scully-Power, 1976; Nilsson and Cresswell, 1980). These energy values place the Agulhas rings as the most energetic rings in the world. Ring E2-94 has the highest initial *APE* and the largest translation speed of about 0.18 m s^{-1} (16 km day^{-1}). Its *APE* value is also larger than any other reported value of this parameter for anticyclonic rings. The initial *APE* value does not seem to be a conclusive factor in the period of time in which these rings can be observed in the region of study (referred from now on as residence time), as both the least energetic, ring E3-93, and most energetic, ring E2-94, cannot be detected for more than two months.

d. Transport and ring formation

i. Baroclinic transport. Altimeter data have already been successfully used to monitor the upper layer transport in the Brazil-Malvinas Confluence region (Goni *et al.,* 1996) and in the Benguela Current (Garzoli *et al.,* 1997). The expression for the upper layer thickness (1) is used here to estimate the baroclinic component of the transport. In the first part of this work the altimeter-derived SHA values produced better estimates of the geostrophic transports in the upper 1000 m than in the upper layer baroclinic transport, with the difference between these two transports being a constant. However, the emphasis in this section is placed on the variability of the transport values and not on the values themselves. Therefore, these two transport estimates provide similar qualitative results.

To compute the baroclinic transport, the bottom layer is assumed to be at rest with changes in the thickness of the upper layer proportional to changes in the sea surface height. The baroclinic transport between two locations a and b is then:

$$S_{cl}(t) = \frac{g'}{2f} \Delta h_1^2(t), \tag{15}$$

where $\Delta h_1^2(t) = h_{1,b}^2(t) - h_{1,a}^2(t)$, and $h_{1,a}^2(t)$, and $h_{1,i}$ is the upper layer thickness at the location i. The baroclinic transport is then a function of the reduced gravity, latitude, and the square of the difference of the upper layer thickness between locations a and b.

The time series for the westward baroclinic transport across 19E for the three year altimeter data computed using (15) is shown in the lower panel of Figure 7. The solid circles in the same figure are placed to indicate the time when the rings are first detected, west of the Retroflection region. Two main features are observed in this figure. First, there are periods of time with very low transport values, such as April until November 1993 and September until December 1994, when there is no ring formation. Second, large incre-

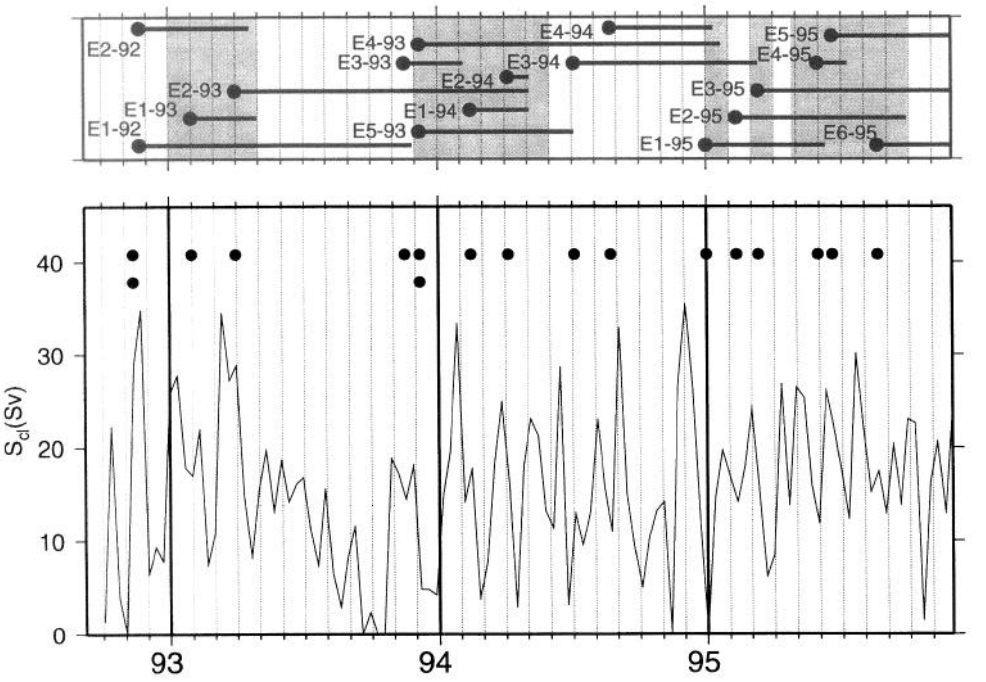

Figure 7. (lower panel) Time series of the upper layer westward baroclinic transport estimates across 19E. The solid circles in this panel show the time when each of the 17 rings are first detected. The shedding of rings from the Agulhas Current seems to be intermittent. (upper panel) Residence times, with the gray areas showing the months when 4 or more rings coexist.

ments in the upper layer transport of the Agulhas Current are usually followed by the formation of anticyclonic rings.

Ring E1-95, which is shed from the Agulhas Current after the largest increase in transport occurred, has the largest h_1 value of all the rings formed during the three year study period. This ring also has one of the fastest translation speeds and reaches the Walvis Ridge in only 5 months after traveling a distance of approximately 1400 km. Although rings E4-93 and E5-93 are formed after the smallest transport variation occurs, they cross the whole region of study and then reach the Walvis Ridge. Ring E3-93 is also formed after very small transport variation. However, this ring, which has a trajectory more to the east than any other ring, can be tracked for only two months. Overall, these results suggest that there is no evidence that the residence time is linked to the upper layer transport variation that formed them.

The panel at the top of Figure 7 shows the residence time for each ring within the region of study between September 1992 and December 1995. The values corresponding to each ring are also shown in the last column of Table 1. The rings with the longest residence time are E1-92, E4-93, E2-93 and E1-92 with 12.5, 13, 13, and 11.5 months, respectively. For example, ring E4-93 is formed at the end of 1993 and remains in the region of study until

the beginning of 1995. This figure also shows that at any given period of time the number of rings in the area ranges from two to six. This number might be actually higher since rings with very small sea height signatures were probably not identified in this study. The shaded areas show the periods of time when four to six rings are simultaneously detected in the region of study. The time series is not long enough to draw a conclusion about any type of periodicity. However, this figure suggests that periods with four or more rings seem to start between December and January and last several months. Moreover, during the last part of each year the figure shows that there are only two or three rings coexisting in the region.

ii. Volume transport of Agulhas rings. The transport of the Benguela Current is estimated to remain almost constant and approximately 14 Sv during the period 1993–1995 (Garzoli *et al.,* 1997). The contribution of the Agulhas waters to the transport of the Benguela Current, mostly in the form of rings and filaments, is estimated to be on the order of 4, 3, and 6 Sv for the years 1993, 1994, and 1995, respectively (Table VII in Garzoli *et al.,* 1997). This result is consistent with the number of rings, 5, 4, and 6, shed by the Agulhas current during 1993, 1994, and 1995, respectively. Two rings, E1-93 and E2-94, do not contribute to the Benguela current transport, as their trajectories end south of 40S. Therefore, if these two rings are excluded, the above result suggests that, on average, every year each ring contributes approximately 1 Sv to the transport of the Benguela Current.

6. Summary and conclusions

In part I of this work TOPEX/POSEIDON data are used in the SE Atlantic Ocean and prove to be a good proxy to estimate the upper layer thickness and transports during the period September 1992–December 1995. The sea-surface height anomaly space-time diagrams provide a useful means to identify the passage of rings across the altimeter groundtracks. These diagrams also reveal that cyclonic and anticyclonic rings possibly alternate their passage across altimeter groundtracks. An objective analysis scheme is used in this work to create upper layer thickness maps to identify, track and compute the speed of 17 warm rings formed in the Agulhas Retroflection region during the same period.

Two major topographic features seem to affect the ring translation region. First, after being formed, rings appear to follow a trajectory parallel to the isobath of 4000 m. Second, the Walvis Ridge seems to split the path of the five rings that reach the ridge into south and north of 30S between 0 and 5E. A ring corridor is obtained from the path of the seventeen warm rings. A close relationship is also found between the axis of the contour of maximum values of altimeter-derived eddy kinetic energy and the ring corridor. None of the rings formed during 1994 appears to reach the Walvis Ridge. Of the five rings that reach the Walvis Ridge during these three years, three cross the Ridge south of 30S and only one north of 30S, the latitude that corresponds to the minimum depth of the Ridge.

The length scale parameters and ring maximum thicknesses are computed from the alongtrack SHA profiles using (2). The horizontal length scales range from 70 to 170 km,

the upper layer thickness from 500 to 750 m, and the speed of translation ranges from 5 to 16 km day^{-1}. Computations of ring volume anomalies indicate that every year about 10^{14} m^3 of additional Indian Ocean waters warmer than 10°C enter the South Atlantic as a consequence of the shedding of rings. The available potential energy is determined by four parameters, the upper layer density, the reduced gravity, the maximum depth of the ring and the ring length scale. The values obtained for the *APE* range from 2 to 71 $\times$ 10^{15} J, confirming that the Agulhas rings are among the most energetic anticyclonic rings.

Ring formation seems to be linked to the Agulhas Current transport across 19E, as large increases in the value of transport are usually followed by the shedding of one or more warm rings. The formation of rings seems to be intermittent, with long periods of time of up to 7 months, such as from April until November 1993, when no rings are shed from the retroflection. At any given time, 2 to 5 warm rings coexist in the region. Periods of time with 4 or 5 rings traveling simultaneously in the region usually start during the southern hemisphere summer. The contribution of each ring to the Benguela Current transport is approximately 1 Sv. Long term monitoring of the formation and the path of the Agulhas rings is necessary to precisely assess the energy and mass contribution of these rings to the Atlantic Ocean.

Acknowledgments. This work was supported by ONR grant N00014-95-1-0166. Support for collection and reduction of the BEST data sets was provided by NSF grant 94-01950, and for the altimeter data, ONR grant N00014-89-1-0166. This research was also supported by NASA and NOAA grants NAF 531361/2 and NA47GPO188. Valuable comments by Dr. Victor Zlotnicki on altimetry and Mrs. Jossy Jacob on the Agulhas ring dynamics helped to improved the manuscript. Dr. Arthur Mariano provided the Objective Analysis computer code to create the upper layer thickness maps. The authors also wish to thank Ms. Miriam Colwell for proofreading the manuscript.

REFERENCES

Andrews, J. C. and P. D. Scully-Power. 1976. The structure of an East Australian Current anticyclonic eddy. J. Phys. Oceanogr., *6,* 756–765.

Byrne, D. A., A. L. Gordon and W. F. Haxby. 1995. Agulhas eddies: A synoptic view using Geosat ERM data. J. Phys. Oceanogr., *25,* 902–917.

Chassignet, E. P., D. B. Olson and D. B. Boudra. 1990. Motion and evolution of oceanic rings in a numerical model and in observations. J. Geophys. Res., *95,* 22,121–22,140.

Dewar, W. K. and G. R. Flierl. 1985. Particle trajectories and simple models of transport in coherent vortices. Dyn. Atmos. Oceans, *9,* 115–152.

Dewar, W. K. and C. Gailliard. 1994. The dynamics of barotropically dominated rings. J. Phys. Oceanogr., *24,* 5–29.

Dewar, W. K. and P. D. Killworth. 1995. On the stability of oceanic rings. J. Phys. Oceanogr., *25,* 1467–1487.

Duncan, C. P. 1965. An eddy in the subtropical convergence southwest of South Africa. J. Geophys. Res., *73,* 531–534.

Duncombe Rae, C. M., S. L. Garzoli, and A. L. Gordon. 1996. The eddy field of the southeast Atlantic Ocean: A statistical census from the Benguela Sources and Transports Project. J. Geophys. Res., *101,* 11,949–11,964.

Duncombe Rae, C. M., F. A. Shillington, J. J. Aagenbag, J. Tauton-Clark and M. L. Gründlingh. 1992. An Agulhas ring in the South Atlantic Ocean and its interaction with the Benguela Upwelling Frontal System. Deep-Sea Res., *39,* 2009–2027.

Feron, R. C. V., W. P. M. de Ruijter and D. Oskman. 1992. Ring shedding in the Agulhas Current system. J. Geophys. Res., *97,* 9467–9477.

Flierl, G. R. 1977. The application of linear quasigeostrophic dynamics to Gulf Stream rings. J. Phys. Oceanogr., *7,* 365–379, 1977.

Garrafo, Z., S. L. Garzoli, W. Haxby and D. Olson. 1992. Analysis of a general circulation model. 2. Distribution of kinetic energy in the South Atlantic and Kuroshio-Oyashio systems. J. Geophys. Res., *97,* 20,139–20,153.

Garzoli, S. L., G. J. Goni, A. J. Mariano and D. B. Olson. 1997. Monitoring the upper Southeastern Atlantic transports using altimeter data. J. Mar. Res., *55,* 453–481.

Garzoli, S. L. and A. L. Gordon. 1996. Origins and variability of the Benguela Current. J. Geophys. Res., *101,* 897–906.

Garzoli, S. L., A. L. Gordon, V. Kamenkovich, D. Pillsbury and C. Duncombe Rae. 1996. Variability and sources of the southeastern Atlantic circulation. J. Mar. Res., *54,* 1039–1071.

Garzoli, S. L., A. L. Gordon and D. Pillsbury. 1994. Initial Results in from BEST Cruises. WOCE Notes, *6,* 1, 10–11, 15.

Goni, G. J., S. Kamholz, S. L. Garzoli and D. B. Olson. 1996. Dynamics of the Brazil-Malvinas Confluence based on inverted echo sounders and altimetry. J. Geophys. Res., *101,* 16,273–16,289.

Gordon, A. L. 1985. Indian Atlantic transfer of thermocline water at the Agulhas Retroflection. Science, *227,* 1030–1033.

Gordon, A. L. and W. F. Haxby. 1990. Agulhas eddies invade the South Atlantic: Evidence from Geosat altimeter and shipboard conductivity-temperature-depth survey. J. Geophys. Res., *95,* 3117–3125.

Gründlingh, M. L. 1995. Tracking eddies in the southeast Atlantic and southwest Indian oceans with TOPEX/POSEIDON. J. Geophys. Res., *100,* 24,977–24,986.

Harris, T. F. W. and D. van Foreest. 1978. Satellite infrared images in the Agulhas Current system. Deep-Sea Res., *25,* 543–548.

Hooker, S. B. and J. W. Brown. 1994. Warm core ring dynamics derived from satellite imagery. J. Geophys. Res., *99,* 25,181–25,234.

Joyce, T. 1984. Velocity and hydrographic structure of a Gulf Stream warm-core ring. J. Phys. Oceanogr., *14,* 936–947.

Kamenkovich, V. M., Y. P. Leonov, D. A. Nechaev, D. A. Byrne and A. L. Gordon. 1996. On the influence of bottom topography on the Agulhas eddy. J. Phys. Oceanogr., *26,* 892–912.

Kelly, K. A. 1991. The meandering of the Gulf Stream as seen by the Geosat altimeter: Surface transport, position, and velocity variance from 73° to 46°W. J. Geophys. Res., *96,* 16,721–16,738.

Levitus, S. and T. P. Boyer. 1994. World Ocean Atlas 1994, Volume 4: Temperature. NOAA Atlas NESDIS 4, 117 pp.

Lutjeharms, J. R. E. 1981. Features of the southern Agulhas Current circulation from satellite remote sensing. S. Afr. J. Sci., *77,* 231–236.

—— 1996. The exchange of water between the South Indian and South Atlantic, *in* The South Atlantic: Present and Past Circulation. G. Wefer, W. H. Berger, G. Siedler, and D. Webb, eds., Springer-Verlag, (in press).

Lutjeharms, J. R. E. and H. R. Valentine. 1988. Eddies at the Subtropical Convergence South of Africa. J. Phys. Oceanogr., *18,* 761–774.

Lutjeharms, J. R. E. and R. C. Van Ballegooyen. 1988. The retroflection of the Agulhas Current. J. Phys. Oceanogr., *18,* 1570–1583.

Mariano, A. J. and O. B. Brown. 1992. Efficient objective analysis of dynamically heterogeneous and nonstationary fields via the parameter matrix. Deep-Sea Res., *39,* 1255–1271.

Mied, R. P. and G. J. Lindemann. 1979. The propagation and evolution of cyclonic Gulf Stream rings. J. Phys. Oceanogr., *9,* 1183–1206.

Nilsson, C. S. and G. R. Cresswell. 1980. The formation and evolution of East Australian Current warm-core eddies. Prog. Oceanogr., *9,* 133–183.

Olson, D. B. 1991. Rings in the ocean. Ann. Rev. Earth Planet. Sci., *19,* 283–311.

Olson, D. B. and R. H. Evans. 1986. Rings of the Agulhas Current. Deep-Sea Res., *33,* 27–42.

Olson, D. B., R. A. Fine and A. L. Gordon. 1992. Convective modifications of water masses in the Agulhas. Deep-Sea Res., *39,* 163–181.

Qui, B. 1992. Recirculation and seasonal change of the Kuroshio from altimetry observations. J. Geophys. Res., *97,* 17,801–17,811.

Van Ballegooyen, R. C., M. L. Gründlingh, and J. R. E. Lutjeharms. 1994. Eddy fluxes of heat and salt from the southwest Indian ocean in the southeast Atlantic Ocean: A case study. J. Geophys. Res., *99,* 14,053–14,070.

Received: *4 March, 1997;* revised: *1 July, 1997.*